

Full NLO corrections to 3-jet production and R_{32} at the LHC

Max Reyer^{a,1,4}, Marek Schönherr^{b,2,3}, Steffen Schumann^{c,4}

¹Albert-Ludwigs-Universität Freiburg, Physikalisches Institut, Hermann-Herder-Straße 3, 79104 Freiburg, Germany

²Theoretical Physics Department, CERN, 1211 Geneva 23, Switzerland

³Institute for Particle Physics Phenomenology, University of Durham, Durham, DH1 3LE, UK

⁴Georg-August-Universität Göttingen, Institut für Theoretische Physik, Friedrich-Hund-Platz 1, 37077 Göttingen, Germany

Received: date / Accepted: date

Abstract We present the evaluation of the complete set of NLO corrections to three-jet production at the LHC. To this end we consider all contributions of $\mathcal{O}(\alpha_s^n \alpha^m)$ with $n + m = 3$ and $n + m = 4$. This includes in particular also subleading Born contributions of electroweak origin, as well as electroweak virtual and QED real-radiative corrections. As an application we present results for the three- over two-jet ratio R_{32} . While the impact of non-QCD corrections on the total cross section is rather small, they can exceed -10% for high jet transverse momenta. The R_{32} observable turns out to be very stable against electroweak corrections, receiving absolute corrections below 5% even in the high- p_T region.

Keywords Hadronic collisions, Jets, Perturbation theory, Radiative Corrections

PACS 13.87.-a, 11.15.Bt, 12.38.Bx, 12.38.Cy, 13.40.Ks, and 12.15.Lk

1 Introduction

Jet-production processes make up the most abundant final states in hadron-hadron collisions, as carried out at the Large Hadron Collider (LHC). They are of great importance for the determination of the strong-coupling constant and provide a central ingredient to precise determinations of parton density functions (PDFs). At the same time pure-jet final states constitute promising search grounds for physics beyond the Standard Model, when looking for resonance peaks or an excess of events in the tails of transverse-momentum-type distributions.

Besides being of high phenomenological relevance, jet-production processes serve as benchmark for various types

of perturbative calculations including fixed-order evaluations, all-orders resummations and parton-shower simulations. Already the two-jet production channel features quarks and gluons in the initial and final states and correspondingly various types of spin- and color-correlations. Beyond the leading order there arise infrared singularities both in the virtual and real corrections that need to be properly treated. Further, sensitivity to the actual jet criterion used to define the cross section emerges. Beyond perturbation theory, there are important corrections from the fragmentation of final-state partons into hadrons and beam-remnant interactions such as multi-parton scatterings.

For hadro-production the next-to-leading order (NLO) QCD corrections are known to up to five-jet final states [1–5]. The computation of the QCD next-to-next-to leading order (NNLO) corrections to dijet production has recently been completed [6], resulting in significantly reduced scale uncertainties in the predictions, paving the way to precision analyses of LHC dijet data. Dedicated studies on the combination of NLO QCD calculations with parton-shower simulations for dijet production have been presented in [7, 8].

To further improve the theoretical accuracy besides QCD also electroweak (EW) corrections need to be considered. A first evaluation of the leading weak corrections to dijet production has been presented in [9]. These included the tree-level contributions of $\mathcal{O}(\alpha_s \alpha)$ and $\mathcal{O}(\alpha^2)$ and weak loop corrections of $\mathcal{O}(\alpha_s^2 \alpha)$. Only recently the complete set of NLO corrections, further including QED virtual and real contributions, was completed [10]. While these corrections are rather small for total cross sections, they can reach 10 – 20% for jet transverse momenta in the TeV range.

A first evaluation of the full set of NLO corrections, of QCD and EW origin, for the three-jet inclusive cross section has been quoted in [11]. In this paper we present results for the fully differential calculation of three-jet production at the LHC to NLO, including all contributions proportional to

^ae-mail: max.reyer@physik.uni-freiburg.de

^be-mail: marek.schoenherr@cern.ch

^ce-mail: steffen.schumann@phys.uni-goettingen.de

$\alpha_s^n \alpha^m$ with $n + m = 3$ and $n + m = 4$. As a first application we consider the observable R_{32} , the ratio of the three-jet and two-jet cross sections, differential in $H_T^{(2)}$, i.e. the scalar sum of the two leading-jets transverse momenta.

Our paper is organised as follows, in Sec. 2 we present our calculational methods and specify our input parameters. In Sec. 3 we present our results for the full NLO calculation of the three-jet process and the R_{32} observable in particular. We give a summary of our findings in Sec. 4.

2 Setup

To obtain the results presented in Sec. 3 we use the SHERPA Monte-Carlo event generator [12] and interface [13] it to RECOLA¹ [14, 15]. Therein, the tree-level matrix elements, infrared subtractions, process management and phase-space integration are provided by SHERPA for all contributions to all processes using its tree-level matrix-element generator AMEGIC [16]. It also implements the infrared subtraction [13, 17–25] in the QCD+QED generalisation of the Catani-Seymour scheme [26–29], including the appropriate initial state mass factorisation counter terms. RECOLA, on the other hand, using the COLLIER library [30] for the evaluation of its scalar and tensor integrals, provides the renormalised virtual corrections.

All calculations are performed in the framework of the Standard Model, assuming a diagonal CKM matrix, and using the five-flavour scheme, i.e. treating the bottom quark as massless. The complex mass scheme [31, 32] is used to consistently treat intermediate resonances in the contributing amplitudes. All electroweak Standard Model parameters are defined in the G_μ -scheme, and virtual amplitudes are renormalised correspondingly. Consequently, the following set of input parameters is used throughout

$$\begin{aligned} G_\mu &= 1.16639 \times 10^{-5} \text{ GeV}^{-2} \\ m_W &= 80.385 \text{ GeV} & \Gamma_W &= 2.085 \text{ GeV} \\ m_Z &= 91.1876 \text{ GeV} & \Gamma_Z &= 2.4952 \text{ GeV} \\ m_h &= 125.0 \text{ GeV} & \Gamma_h &= 0.00407 \text{ GeV} \\ m_t &= 173.21 \text{ GeV} & \Gamma_t &= 1.3394 \text{ GeV}. \end{aligned}$$

All other masses and widths are set to zero. In the above,

$$\alpha = \left| \frac{\sqrt{2} G_\mu \mu_W^2 \sin^2 \theta_w}{\pi} \right|, \quad (1)$$

defines the electromagnetic coupling. The complex mass of particle i and the weak mixing angle are defined according to

$$\mu_i^2 = m_i^2 - im_i \Gamma_i \quad \text{and} \quad \sin^2 \theta_w = 1 - \frac{\mu_W^2}{\mu_Z^2}, \quad (2)$$

¹ The public version 1.2 of RECOLA is used.

respectively.

For the parton density functions we use the NNPDF3.1 NLO PDF set [33] with $\alpha_s(m_Z) = 0.118$ and including QED effects (at $\mathcal{O}(\alpha)$, $\mathcal{O}(\alpha_s \alpha)$ and $\mathcal{O}(\alpha^2)$) in the parton evolution employing the LUXqed scheme [34, 35]². They are interfaced through LHAPDF [36]. The renormalisation and factorisation scales are defined as

$$\mu_R = \mu_F = \frac{1}{2} \hat{H}_T. \quad (3)$$

The variable \hat{H}_T is thereby given by the scalar sum of all final-state particles' transverse momenta without applying any jet clustering. To estimate the uncertainty on our computation from uncalculated higher-order contributions, we vary the renormalisation and factorisation scales independently by the customary factor two, keeping $\frac{1}{2} \leq \mu_R/\mu_F \leq 2$. All scale variations were calculated on-the-fly using the event-reweighting algorithm detailed in [37].

3 Results

In this section numerical results for the production of a three-jet final state at next-to-leading order accuracy in proton-proton collisions at a centre-of-mass energy of 13 TeV are presented. We generate the respective matrix elements at all contributing orders for all partonic processes with massless three (Born and virtual corrections) and four body final states (real corrections). As final-state particles we consider five quark flavours and gluons, as well as photons, leptons and neutrinos. Jets are then defined through the anti- k_t algorithm [38] using FASTJET [39], with $R = 0.4$ as radial parameter. All massless particles of our calculation, except for the neutrinos, are considered as jet constituents. Jets with a net lepton number³ and within $|\eta| < 2.5$ are removed from the list of jets. The final state then has to contain at least three surviving jets with $|\eta(j)| < 2.8$, of which the leading jet, ordered in transverse momentum, must have $p_T(j_1) > 80 \text{ GeV}$ and all subleading jets $p_T(j_i) > 60 \text{ GeV}$ ($i > 1$). This ensures that a jet definition with inherent lepton rejection, which is both infrared-safe at NLO and close to experimental analysis strategies, is used. Nonetheless, it is worth pointing out that lepton final states may survive this lepton-anti-tagged jet definition if either a collinear lepton pair is contained in a single jet (possibly coming from a collinear $\gamma \rightarrow \ell^+ \ell^-$ splitting), or the jet containing the lepton is outside the rapidity range in which the lepton can be identified. To analyse our results we use the RIVET package [40].

The full NLO n -jet production cross section can be decomposed into contributions of varying power of the strong

² To be precise the NNPDF31_nlo_as_0118_luxqed PDF set is used.

³ A jet with a lepton and an anti-lepton, if they are of the same lepton flavour, has net lepton number zero.

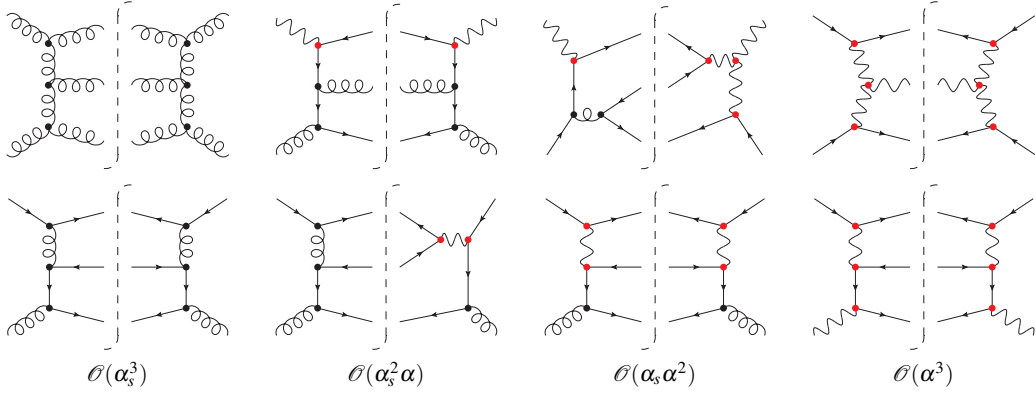


Fig. 1 Representative leading and subleading tree-level diagrams for $pp \rightarrow 3j$ production. The occurrence of QCD and electroweak interferences, internal electroweak bosons and external photons (wavy lines) in the initial and final state are exemplified. While QCD vertices are marked by a black dot, EW interactions are indicated in red.

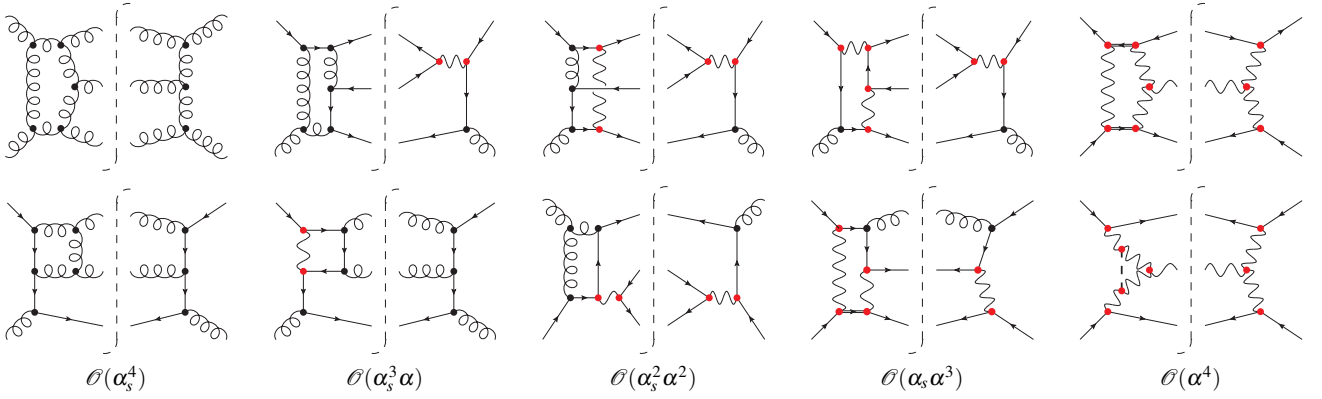


Fig. 2 Representative leading and subleading virtual correction diagrams for $pp \rightarrow 3j$ production. The occurrence of interferences, QCD and EW loops, gauge boson (wavy line), Higgs boson (dashed line) and top quark (double line) exchange as well as external photons are exemplified. While QCD vertices are marked by a black dot, EW interactions are indicated in red.

and electromagnetic coupling. In what follows we employ the convention:

$$\begin{aligned} \sigma_{nj} &= \sigma_{nj}^{\text{LO}} + \sigma_{nj}^{\Delta\text{NLO}}, \\ \sigma_{nj}^{\text{LO}} &= \sum_{i=0}^n \sigma_{nj}^{\text{LO}_i}, & \theta(\sigma_{nj}^{\text{LO}_i}) &= \alpha_s^{n-i} \alpha^i, \\ \sigma_{nj}^{\Delta\text{NLO}} &= \sum_{i=0}^{n+1} \sigma_{nj}^{\Delta\text{NLO}_i}, & \theta(\sigma_{nj}^{\Delta\text{NLO}_i}) &= \alpha_s^{n+1-i} \alpha^i, \end{aligned} \quad (4)$$

such that ΔNLO_i accounts for the virtual and real QCD corrections while ΔNLO_{i+1} accounts for the virtual and real electroweak corrections to LO_i . Representative diagrams for the various tree-level and virtual contributions can be found in Fig. 1 and Fig. 2, respectively. It is worth noting that our full NLO calculation in the five-flavour scheme is indeed sensitive to the full Standard Model spectrum, including the top-quark, the Higgs boson and all lepton and neutrino flavours.

Based on the above decomposition we can furthermore define the pure QCD LO and NLO cross sections as

$$\begin{aligned} \sigma_{nj}^{\text{LO QCD}} &= \sigma_{nj}^{\text{LO}_0}, \\ \sigma_{nj}^{\text{NLO QCD}} &= \sigma_{nj}^{\text{LO}_0} + \sigma_{nj}^{\Delta\text{NLO}_0}, \end{aligned} \quad (5)$$

respectively. The pure NLO EW corrections and their additive and multiplicative combination with the QCD process are defined as

$$\begin{aligned} \sigma_{nj}^{\text{NLO EW}} &= \sigma_{nj}^{\text{LO}_0} + \sigma_{nj}^{\Delta\text{NLO}_1}, \\ \sigma_{nj}^{\text{NLO QCD+EW}} &= \sigma_{nj}^{\text{LO}_0} + \sigma_{nj}^{\Delta\text{NLO}_0} + \sigma_{nj}^{\Delta\text{NLO}_1}, \\ \sigma_{nj}^{\text{NLO QCD}\times\text{EW}} &= \sigma_{nj}^{\text{LO}_0} \left(1 + \frac{\sigma_{nj}^{\Delta\text{NLO}_0}}{\sigma_{nj}^{\text{LO}_0}} \right) \left(1 + \frac{\sigma_{nj}^{\Delta\text{NLO}_1}}{\sigma_{nj}^{\text{LO}_0}} \right). \end{aligned} \quad (6)$$

The difference between the additive and multiplicative combination provides an estimate of uncalculated mixed QCD-EW NNLO corrections of $\theta(\alpha_s \alpha)$, wrt. LO QCD.

We start our discussion of results by listing the inclusive two- and three-jet cross sections for leading-jet selections of $p_T(j_1) > 80 \text{ GeV}$ and $p_T(j_1) > 2 \text{ TeV}$ in Tables 1 and 2, respectively. We quote results at full NLO accuracy in the Standard Model and list their decomposition into all contributing orders. The numbers quoted in parentheses indicate the statistical error estimate on the last digit given. For

	NLO	$\frac{LO_0}{NLO}$	$\frac{LO_1}{NLO}$	$\frac{LO_2}{NLO}$	$\frac{LO_3}{NLO}$	$\frac{\Delta NLO_0}{NLO}$	$\frac{\Delta NLO_1}{NLO}$	$\frac{\Delta NLO_2}{NLO}$	$\frac{\Delta NLO_3}{NLO}$	$\frac{\Delta NLO_4}{NLO}$
	[nb]	[%]	[%]	[%]	[%]	[%]	[%]	[%]	[%]	[%]
σ_{2j}	3385(3)	67.34(6)	0.0713(1)	0.03915(4)	–	32.59(8)	–0.118(7)	0.0759(3)	0.00022(1)	–
σ_{3j}	169(1)	148(1)	0.293(2)	0.196(2)	0.00217(2)	–48.4(8)	–0.74(1)	0.344(7)	–0.00433(6)	0.0135(2)

Table 1 Full NLO fiducial cross section for two- and three-jet production in the phase space detailed in the text, i.e. $p_T(j_1) > 80$ GeV and $p_T(j_i) > 60$ GeV ($i > 1$). Besides the total cross section the relative contributions for the terms specified in Eqs. (4) are given.

	NLO	$\frac{LO_0}{NLO}$	$\frac{LO_1}{NLO}$	$\frac{LO_2}{NLO}$	$\frac{LO_3}{NLO}$	$\frac{\Delta NLO_0}{NLO}$	$\frac{\Delta NLO_1}{NLO}$	$\frac{\Delta NLO_2}{NLO}$	$\frac{\Delta NLO_3}{NLO}$	$\frac{\Delta NLO_4}{NLO}$
	[fb]	[%]	[%]	[%]	[%]	[%]	[%]	[%]	[%]	[%]
σ_{2j}	51.9(6)	60(1)	7.07(8)	1.82(2)	–	36.9(8)	–4.5(1)	–1.02(2)	–0.552(7)	–
σ_{3j}	40.0(4)	99(1)	8.6(1)	2.05(4)	0.061(1)	–0.9(9)	–9.8(4)	1.09(7)	0.057(4)	0.314(5)

Table 2 As Table 1 but with the additional requirement of $p_T(j_1) > 2$ TeV.

	NLO	LO QCD	NLO QCD	NLO EW	NLO QCD + EW
	[nb]	[nb]	[nb]	[nb]	[nb]
σ_{2j}	3385(3) $^{+334}_{-338}$	2279.4(6) $^{+553.7}_{-404.4}$	3383(3) $^{+335}_{-338}$	2275.4(6) $^{+552.4}_{-403.5}$	3379(3) $^{+333}_{-338}$
σ_{3j}	169(1) $^{+16}_{-73}$	249.86(6) $^{+102.28}_{-67.89}$	168(1) $^{+16}_{-73}$	248.62(6) $^{+101.62}_{-67.46}$	167(1) $^{+17}_{-73}$

Table 3 Fiducial cross sections for two- and three-jet production and their corresponding scale uncertainties for a leading-jet selection of $p_T(j_1) > 80$ GeV. The respective cross section definitions are given in Eqs. (5) and (6).

	NLO	LO QCD	NLO QCD	NLO EW	NLO QCD + EW
	[fb]	[fb]	[fb]	[fb]	[fb]
σ_{2j}	51.9(6) $^{+5.9}_{-6.7}$	31.2(5) $^{+11.4}_{-7.9}$	50.4(6) $^{+7.1}_{-7.3}$	28.9(5) $^{+9.6}_{-6.7}$	48.1(6) $^{+5.2}_{-6.1}$
σ_{3j}	40.0(4) $^{+0.4}_{-6.9}$	39.4(2) $^{+19.0}_{-12.1}$	39.0(4) $^{+0.0}_{-5.0}$	35.5(2) $^{+15.7}_{-10.2}$	35.1(4) $^{+0.9}_{-8.2}$

Table 4 As Table 3 but with the additional requirement of $p_T(j_1) > 2$ TeV.

a leading jet requirement of $p_T(j_1) > 80$ GeV corrections of EW origin are generally rather small, reaching for the three-jet case at most a relative contribution to the full NLO result of -0.7% for ΔNLO_1 . The dominant corrections are of QCD nature and account for $+33\%$ and -48% for two- and three-jet production, respectively.

Requiring $p_T(j_1) > 2$ TeV changes the picture. While for the two-jet process the QCD NLO corrections are still dominating, amounting to $+37\%$, QCD-EW mixed Born and EW one-loop contributions clearly become sizeable, though they largely cancel. For three-jet production in this selection and scale choice the NLO QCD corrections are, accidentally, miniscule, below -1% . However, the Born contributions of EW origin reach a total of $+11\%$ but largely get cancelled by the ΔNLO_1 terms that contribute -10% to the total NLO result.

In Tables 3 and 4 we quote two- and three-jet cross sections at full NLO, LO QCD, NLO QCD, NLO EW and NLO QCD + EW for the leading-jet selections of $p_T(j_1) > 80$ GeV and $p_T(j_1) > 2$ TeV, respectively. Besides the nom-

inal cross sections we give their scale uncertainty estimates obtained from 7-point variations around the central scale choice $\mu_R = \mu_F = \frac{1}{2} \hat{H}_T$. A significant reduction in particular of the upward variations wrt. LO QCD is observed for predictions including the ΔNLO_0 terms. Adding the ΔNLO_1 corrections, however, has no sizeable effect on the scale uncertainties. Furthermore, no systematic reduction of the scale uncertainties of the full NLO results in comparison to the NLO QCD + EW predictions is observed.

In principle, the addition of a $p_T > 2$ TeV requirement on the leading jet, while leaving the subleading jets at $p_T > 60$ GeV only, introduces a large scale hierarchy to cross section results presented in Tables 2 and 4. In principle, this mandates the inclusion of a resummation of the corresponding potentially large logarithms. However, no perturbative instabilities were encountered in this region and we, thus, consider the results reliable. Similar considerations, of course, also apply to the tails of the distributions shown in the following.

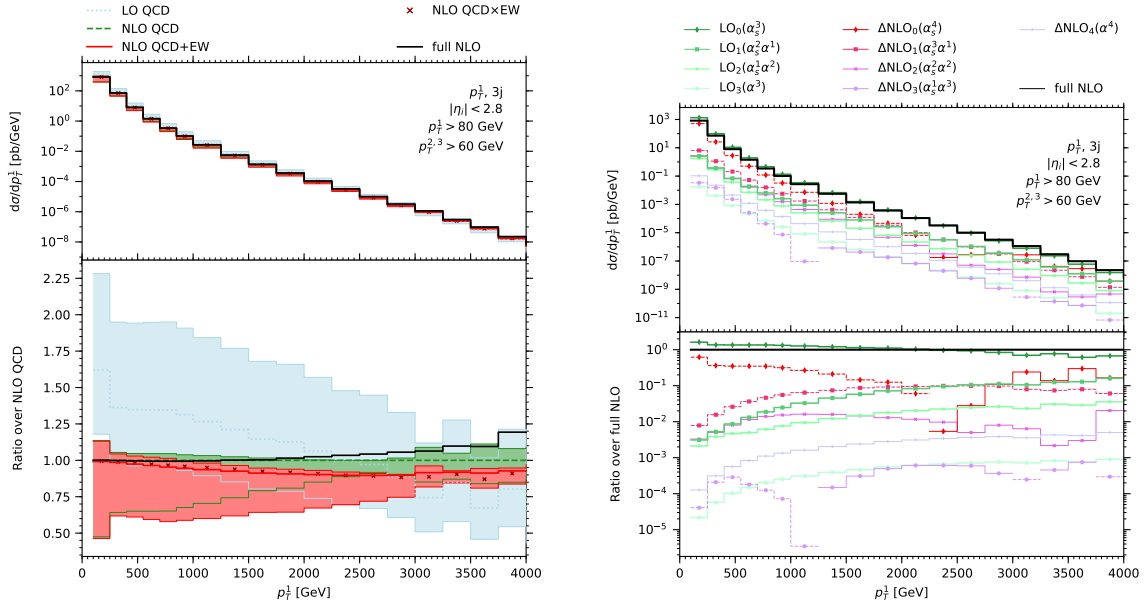


Fig. 3 Leading jet transverse momentum in three-jet production. Left: Theoretical uncertainties at LO, NLO QCD, NLO QCD+EW and full NLO. Right: Decomposition of the full NLO result in its contributions defined in Eqs. (4).

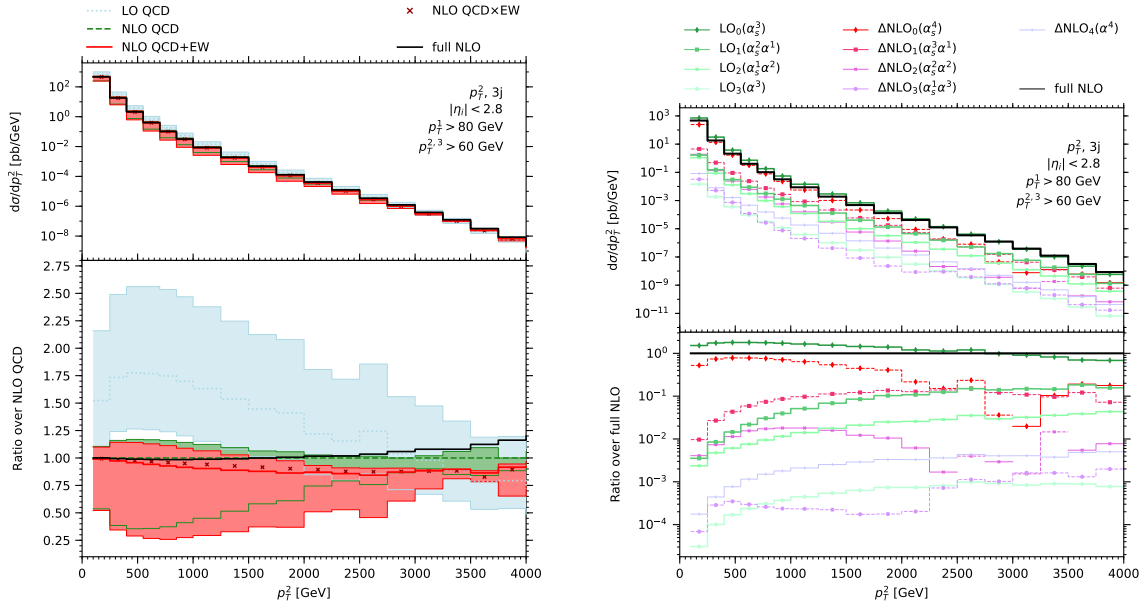


Fig. 4 Subleading jet transverse momentum in three-jet production. Left: Theoretical uncertainties at LO, NLO QCD, NLO QCD+EW and full NLO. Right: Decomposition of the full NLO result in its contributions defined in Eqs. (4).

Figures 3–5 show the three-jet cross section differential in the transverse momentum of the leading, subleading and third hardest jet, respectively. The left hand side panel details the scale uncertainties and relative magnitudes of the LO QCD, the NLO QCD + EW, the NLO QCD × EW and the complete NLO (full NLO) result in comparison to the NLO QCD prediction. Similarly, the right hand side panel details the relative contributions from the various LO and

NLO contributions to the full NLO result for the central scale choice. Note, while positive sub-contributions are represented by a solid line, negative parts are indicated by a dashed line and their corresponding absolute value is displayed here.

In all three distributions we confirm the substantial shape correction and improvement on the scale uncertainty through the NLO QCD corrections observed in earlier calculations

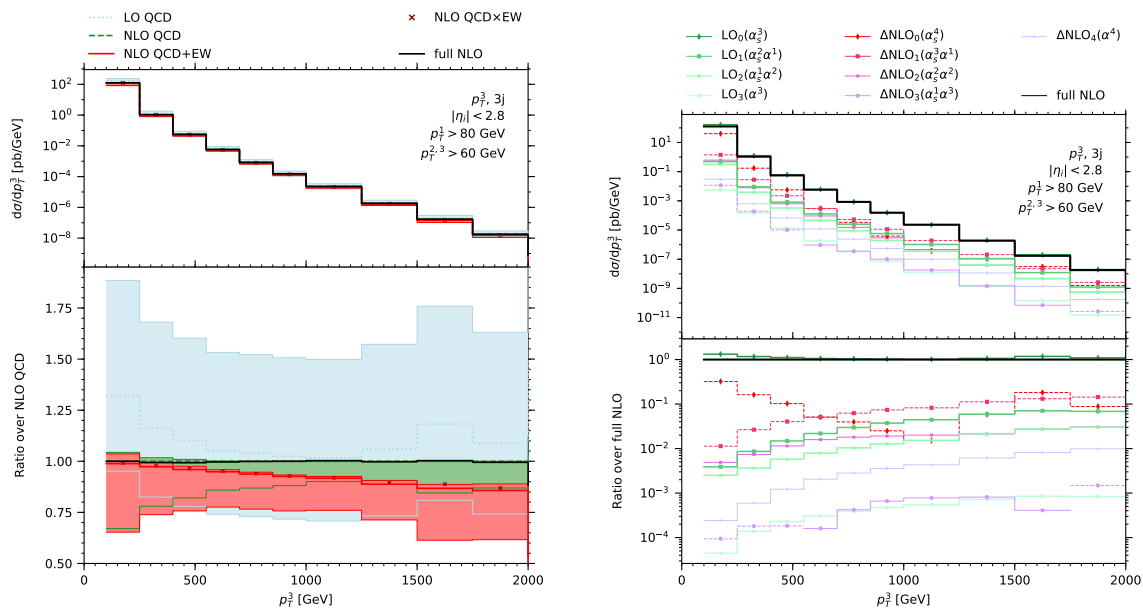


Fig. 5 Third jet transverse momentum in three-jet production. Left: Theoretical uncertainties at LO, NLO QCD, NLO QCD+EW and full NLO. Right: Decomposition of the full NLO result in its contributions defined in Eqs. (4).

of these quantities [3]. The NLO EW corrections themselves lead to the well-known negative corrections of EW Sudakov-type in the high-transverse momentum regime, reaching -10% for the leading, -15% for the second and -15% for the third hardest jet at $p_T = 2$ TeV. The very good agreement of the additive and multiplicative combination of QCD and electroweak corrections indicates a negligible size of the relative $\mathcal{O}(\alpha_s\alpha)$ corrections. The remaining subleading LO and NLO contributions, however, cancel the effect of the next-to-leading order electroweak corrections almost completely. In fact, at $p_T > 2.5$ TeV they grow larger and increase the full NLO result beyond the NLO QCD one. The driving ingredients here are the $\mathcal{O}(\alpha_s^3\alpha)$ Δ NLO₁ terms, the tree-level interference $\mathcal{O}(\alpha_s^2\alpha)$ (LO₁) contributions, followed by the interference at $\mathcal{O}(\alpha_s\alpha^2)$ (LO₂) and their respective EW and QCD corrections at $\mathcal{O}(\alpha_s^2\alpha^2)$ (Δ NLO₂). All other contributions to the full NLO result remain marginal. It has to be stressed that this cancellation is accidental and highly observable dependent and cannot be inferred to hold for any other observable, or indeed for the same observable in a different fiducial phase space. Lastly we note, that by the inclusion of NLO EW corrections the uncertainty estimates obtained by QCD scale variations increases wrt. the NLO QCD result, however, still being significantly smaller than for the LO QCD prediction.

Figure 6 now displays the results for the scalar sum of the leading and subleading jet transverse momenta, $H_T^{(2)}$, in two- and three-jet events. While the latter represents a novel result from our full NLO three-jet calculation, the first is obtained from a dijet computation with identical parameter

settings, scale choices and PDFs. Qualitatively, the $H_T^{(2)}$ distributions exhibit the same features as the leading and sub-leading jet transverse momentum distributions presented before. While the scale uncertainties are shrunk going from LO to NLO QCD, the electroweak corrections show the expected Sudakov behaviour. The relative electroweak corrections are of nearly the same magnitude for both the two- and the three-jet case. This can be understood from the fact that with $H_T^{(2)}$ in the TeV region, where the electroweak corrections become sizeable, the additional third jet in the three-jet case is predominantly soft and near the jet threshold. In this limit, higher order QCD and EW corrections should factorise. Further, we note that for both distributions the additive and multiplicative combination of NLO QCD and EW corrections give compatible results. As has been observed before in the jet transverse momenta, including electroweak contributions somewhat increases the uncertainty wrt. NLO QCD.

Upon inclusion of the additional subleading LO and NLO contributions NLO EW effects get cancelled and the full NLO result gets very close to the NLO QCD prediction. Interestingly, this is true both for the two- and three-jet case. However, this cancellation is accidental and highly dependent on the observable and the phase space considered. To illustrate this observation, Figure 7 shows the same observable, $H_T^{(2)}$, in different regions of absolute pseudorapidity of the leading two-jet system, i.e. $\eta = |\eta_1 - \eta_2|/2$. In the central region, which dominates the inclusive result, the sub-leading contributions, dominated by LO₁ in both the two- and three-jet case, have a large positive effect on the cross

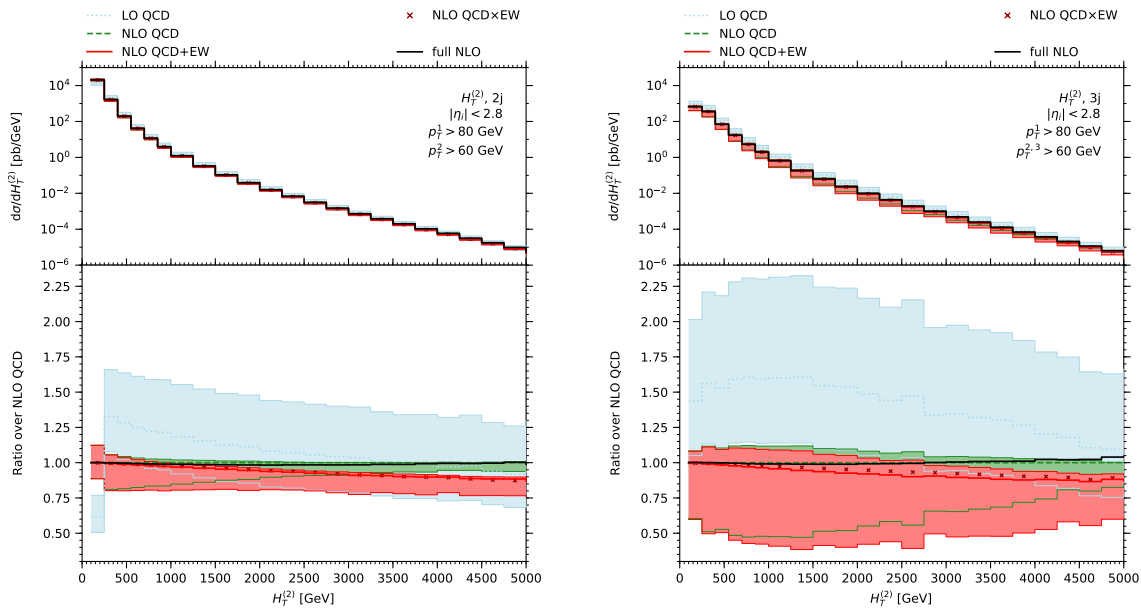


Fig. 6 The $H_T^{(2)}$ distribution in two- and three-jet production at the LHC shown in the left and right panel, respectively. Besides the full NLO prediction the central results and scale uncertainty bands for LO and NLO QCD, NLO QCD + EW and NLO QCD + EW are shown.

section. The more forward $H_T^{(2)}$ is considered, however, the smaller especially the LO₁ terms become and the closer the full NLO result is to the NLO QCD + EW one. This was already observed in [9]. In this region, also qualitative differences between the two- and three-jet case are apparent. While the further subleading contributions are negative wrt. the NLO QCD + EW result in the dijet case, they are positive wrt. the NLO QCD + EW result in the three-jet case.

With full NLO calculations for two- and three-jet production at hand we turn to the central observable of this letter, the three-jet-over-two-jet ratio, R_{32} . This particular observable has attracted interest, as large parts of the experimental and theoretical uncertainties in the inclusive three- and two-jet cross sections cancel in the ratio, allowing for a competitive measurement of the strong coupling α_s [41, 42]. Here we consider R_{32} differential in $H_T^{(2)}$, the scalar sum of the leading- and subleading-jet transverse momenta presented above, i.e.

$$R_{32}(H_T^{(2)}) = \frac{d\sigma_{3j}/dH_T^{(2)}}{d\sigma_{2j}/dH_T^{(2)}}. \quad (7)$$

The scale uncertainties are computed by synchronous variations of numerator and denominator. Our results are presented in Figure 8.

We find that as the individual input distributions receive only minute EW corrections, resulting in the NLO QCD predictions to agree with the full NLO, also their ratio is very stable. However, as emphasised before, accidental cancellations of individually much larger terms is in action for this

observable. Therefore, we present in Figure 9 results differential in various pseudorapidity regions, with $\eta = |\eta_1 - \eta_2|/2$. As before, the inclusive result is dominated by the most central pseudorapidity slices, and they exhibit the same characteristics. In the slightly more forward regions, between $0.5 \leq \eta \leq 2$, the input distributions of Figure 7 do not exhibit this almost complete cancellation of corrections any longer.

For the cross-section ratio R_{32} the net effect is nonetheless the same and the residual corrections of electroweak and subleading origin are very small. Their contributions largely factorise in the numerator and denominator and, thus, cancel in the ratio. Hence, the full NLO result is in very good agreement with the NLO QCD prediction for this observable. This very much confirms the particular usefulness of R_{32} for the determination of the strong coupling.

4 Conclusions

In this letter we have presented the evaluation of the full set of Standard Model NLO corrections to three-jet production at the LHC. Besides the dominating QCD corrections of $\mathcal{O}(\alpha_s^4)$ this comprises all (mixed) electroweak tree-level contributions up to $\mathcal{O}(\alpha^3)$ as well as all (mixed) one-loop and real-corrections up to $\mathcal{O}(\alpha^4)$. As jet constituents we consider besides quarks and gluons also photons and charged leptons. However, for the considered event selections contributions from final states containing leptons are practically irrelevant. All calculations have been performed in an automated manner within the SHERPA event genera-

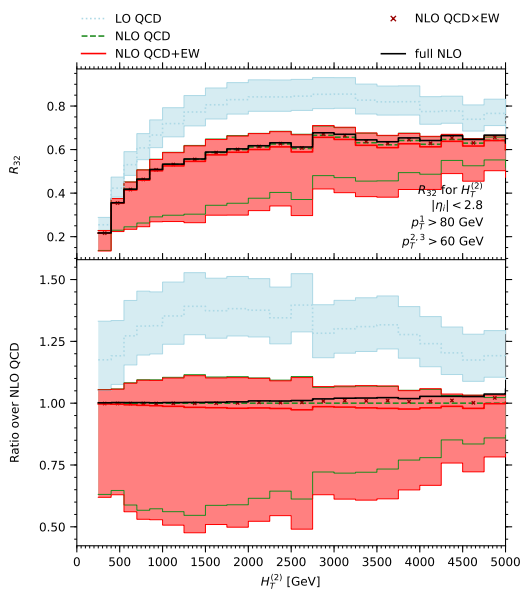


Fig. 8 The R_{32} observable differential in $H_T^{(2)}$. Upper panel: Predictions at LO and NLO QCD, NLO QCD + EW, NLO QCD \times EW and full NLO in the Standard Model. Lower panel: Related relative corrections wrt. the central NLO QCD result.

part of the Marie Skłodowska-Curie Innovative Training Network MC-netITN3 (grant agreement no. 722104). SS acknowledges support through the Fulbright-Cottrell Award and from BMBF (contracts 05H15MGCAA and 05H18MGCA1). MS acknowledges the support of the Royal Society through the award of a University Research Fellowship. MR is supported by the Research Training Group GRK 2044 of the German Research Foundation (DFG).

References

1. S.D. Ellis, Z. Kunszt, D.E. Soper, Phys. Rev. Lett. **69**, 1496 (1992). DOI 10.1103/PhysRevLett.69.1496
2. W.T. Giele, E.W.N. Glover, D.A. Kosower, Nucl. Phys. **B403**, 633 (1993). DOI 10.1016/0550-3213(93)90365-V
3. Z. Nagy, Phys. Rev. **D68**, 094002 (2003). DOI 10.1103/PhysRevD.68.094002
4. Z. Bern, G. Diana, L.J. Dixon, F. Febres Cordero, S. Höche, D.A. Kosower, H. Ita, D. Maitre, K. Ozeren, Phys. Rev. Lett. **109**, 042001 (2012). DOI 10.1103/PhysRevLett.109.042001
5. S. Badger, B. Biedermann, P. Uwer, V. Yundin, Phys. Rev. **D89**(3), 034019 (2014). DOI 10.1103/PhysRevD.89.034019
6. J. Currie, A. Gehrmann-De Ridder, T. Gehrmann, E.W.N. Glover, A. Huss, J. Pires, Phys. Rev. Lett. **119**(15), 152001 (2017). DOI 10.1103/PhysRevLett.119.152001
7. S. Alioli, K. Hamilton, P. Nason, C. Oleari, E. Re, JHEP **04**, 081 (2011). DOI 10.1007/JHEP04(2011)081
8. S. Höche, M. Schönherr, Phys. Rev. **D86**, 094042 (2012). DOI 10.1103/PhysRevD.86.094042
9. S. Dittmaier, A. Huss, C. Speckner, JHEP **11**, 095 (2012). DOI 10.1007/JHEP11(2012)095
10. R. Frederix, S. Frixione, V. Hirschi, D. Pagani, H.S. Shao, M. Zaro, JHEP **04**, 076 (2017). DOI 10.1007/JHEP04(2017)076
11. R. Frederix, S. Frixione, V. Hirschi, D. Pagani, H.S. Shao, M. Zaro, JHEP **07**, 185 (2018). DOI 10.1007/JHEP07(2018)185
12. T. Gleisberg, S. Höche, F. Krauss, M. Schönherr, S. Schumann, F. Siegert, J. Winter, JHEP **02**, 007 (2009). DOI 10.1088/1126-6708/2009/02/007
13. B. Biedermann, S. Bräuer, A. Denner, M. Pellen, S. Schumann, J.M. Thompson, Eur. Phys. J. **C77**, 492 (2017). DOI 10.1140/epjc/s10052-017-5054-8
14. S. Actis, A. Denner, L. Hofer, A. Scharf, S. Uccirati, JHEP **04**, 037 (2013). DOI 10.1007/JHEP04(2013)037
15. S. Actis, A. Denner, L. Hofer, J.N. Lang, A. Scharf, S. Uccirati, Comput. Phys. Commun. **214**, 140 (2017). DOI 10.1016/j.cpc.2017.01.004
16. F. Krauss, R. Kuhn, G. Soff, JHEP **02**, 044 (2002). DOI 10.1088/1126-6708/2002/02/044
17. T. Gleisberg, F. Krauss, Eur. Phys. J. **C53**, 501 (2008). DOI 10.1140/epjc/s10052-007-0495-0
18. M. Schönherr, Eur. Phys. J. **C78**(2), 119 (2018). DOI 10.1140/epjc/s10052-018-5600-z
19. S. Kallweit, J.M. Lindert, P. Maierhöfer, S. Pozzorini, M. Schönherr, JHEP **04**, 012 (2015). DOI 10.1007/JHEP04(2015)012
20. S. Kallweit, J.M. Lindert, P. Maierhöfer, S. Pozzorini, M. Schönherr, JHEP **04**, 021 (2016). DOI 10.1007/JHEP04(2016)021
21. S. Kallweit, J.M. Lindert, S. Pozzorini, M. Schönherr, JHEP **11**, 120 (2017). DOI 10.1007/JHEP11(2017)120
22. M. Chiesa, N. Greiner, M. Schönherr, F. Tramontano, JHEP **10**, 181 (2017). DOI 10.1007/JHEP10(2017)181
23. N. Greiner, M. Schönherr, JHEP **01**, 079 (2018). DOI 10.1007/JHEP01(2018)079
24. C. Gütschow, J.M. Lindert, M. Schönherr, Eur. Phys. J. **C78**(4), 317 (2018). DOI 10.1140/epjc/s10052-018-5804-2
25. M. Schönherr, JHEP **07**, 076 (2018). DOI 10.1007/JHEP07(2018)076
26. S. Catani, M.H. Seymour, Nucl. Phys. **B485**, 291 (1997). DOI 10.1016/S0550-3213(96)00589-5. [Erratum: Nucl. Phys. **B510**, 503(1998)]
27. S. Dittmaier, Nucl. Phys. **B565**, 69 (2000). DOI 10.1016/S0550-3213(99)00563-5
28. S. Catani, S. Dittmaier, M.H. Seymour, Z. Trocsanyi, Nucl. Phys. **B627**, 189 (2002). DOI 10.1016/S0550-3213(02)00098-6

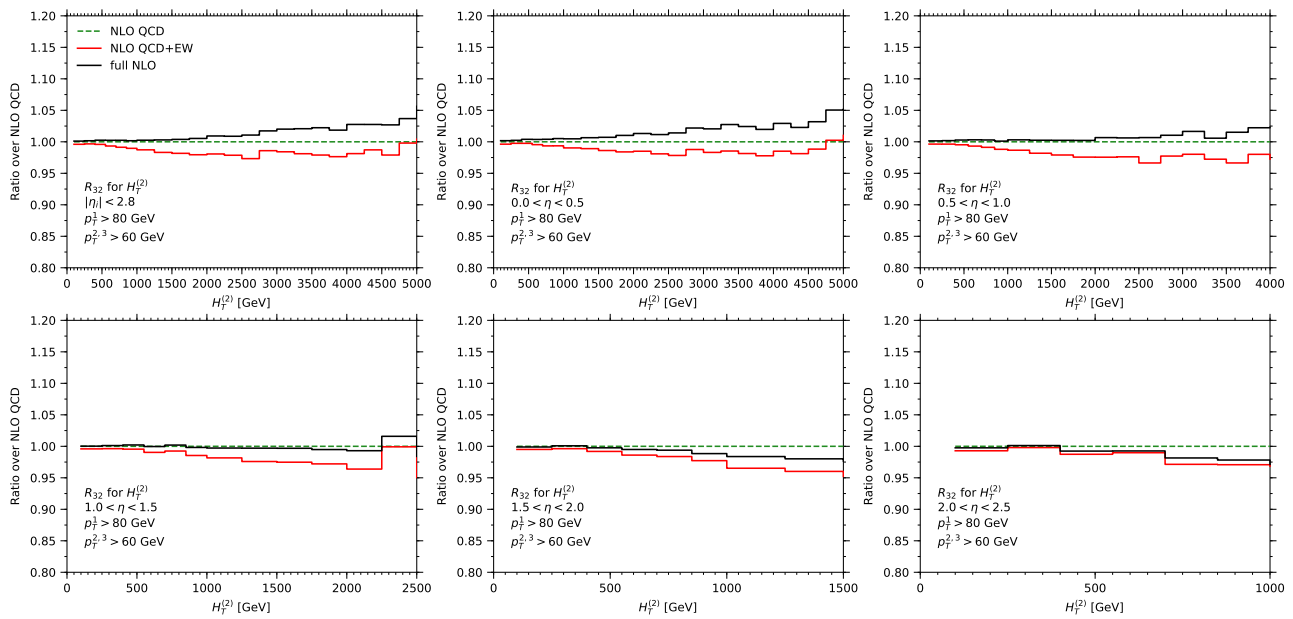


Fig. 9 The R_{32} observable at NLO QCD + EW and full NLO differential in $H_1^{(2)}$ for different pseudo-rapidity selections and in comparison to the corresponding NLO QCD result.

29. S. Dittmaier, A. Kabelschacht, T. Kasprzik, Nucl. Phys. **B800**, 146 (2008). DOI 10.1016/j.nuclphysb.2008.03.010
30. A. Denner, S. Dittmaier, L. Hofer, Comput. Phys. Commun. **212**, 220 (2017). DOI 10.1016/j.cpc.2016.10.013
31. A. Denner, S. Dittmaier, M. Roth, L.H. Wieders, Nucl. Phys. **B724**, 247 (2005). DOI 10.1016/j.nuclphysb.2011.09.001, 10.1016/j.nuclphysb.2005.06.033. [Erratum: Nucl. Phys. **B854**, 504 (2012)]
32. A. Denner, J.N. Lang, Eur. Phys. J. **C75**(8), 377 (2015). DOI 10.1140/epjc/s10052-015-3579-2
33. V. Bertone, S. Carrazza, N.P. Hartland, J. Rojo, SciPost Phys. **5**(1), 008 (2018). DOI 10.21468/SciPostPhys.5.1.008
34. A. Manohar, P. Nason, G.P. Salam, G. Zanderighi, Phys. Rev. Lett. **117**(24), 242002 (2016). DOI 10.1103/PhysRevLett.117.242002
35. A.V. Manohar, P. Nason, G.P. Salam, G. Zanderighi, JHEP **12**, 046 (2017). DOI 10.1007/JHEP12(2017)046
36. A. Buckley, J. Ferrando, S. Lloyd, K. Nordström, B. Page, M. Rüfenacht, M. Schönherr, G. Watt, Eur. Phys. J. **C75**(3), 132 (2015). DOI 10.1140/epjc/s10052-015-3318-8
37. E. Bothmann, M. Schönherr, S. Schumann, Eur. Phys. J. **C76**(11), 590 (2016). DOI 10.1140/epjc/s10052-016-4430-0
38. M. Cacciari, G.P. Salam, G. Soyez, JHEP **04**, 063 (2008). DOI 10.1088/1126-6708/2008/04/063
39. M. Cacciari, G.P. Salam, G. Soyez, Eur. Phys. J. **C72**, 1896 (2012). DOI 10.1140/epjc/s10052-012-1896-2
40. A. Buckley, J. Butterworth, L. Lönnblad, D. Grellscheid, H. Hoeth, J. Monk, H. Schulz, F. Siegert, Comput. Phys. Commun. **184**, 2803 (2013). DOI 10.1016/j.cpc.2013.05.021
41. G. Aad, et al., Eur. Phys. J. **C71**, 1763 (2011). DOI 10.1140/epjc/s10052-011-1763-6
42. S. Chatrchyan, et al., Eur. Phys. J. **C73**(10), 2604 (2013). DOI 10.1140/epjc/s10052-013-2604-6